Journal of Computer Science and Technological Enquiry 2(02) (2026)

Contents lists available at Noesis Publishing

Journal of Computer Science and Technological Enquiry

journal homepage: https://journals.noesispub.com/jcste

Research paper

Improved Median Filtering for Image Denoising

Yuqing Liu[a], Lei Yan[a], Xinyu Dong[a], Li Li[a*], Yufeng Wang[a], Jianqiang Gao[a*], Xiu Liu[b]

[a] *School of Medical Information Engineering, Jining Medical University, Rizhao 276800, Shandong, China*

[b] *Department of Ultrasound Medicine, Yantai Affiliated Hospital of Shandong Medical and Pharmaceutical University, Yantai 264100, Shandong, China*

A R T I C L E I N F O

Keywords:
Image Denoising
Salt-and-Pepper Noise
Improved Median Filter
Adaptive Threshold
Local Statistical Characteristics

A B S T R A C T

Traditional median filters easily blur fine textures and weaken edge definition during salt-and-pepper noise elimination. To tackle this limitation, this paper proposes an improved median filter integrated with adaptive thresholds and local statistical features. The algorithm firstly classifies the central pixel as an extreme point or ordinary pixel. For extreme pixels, median values and adaptive thresholds are computed only from valid non-extreme pixels inside the filtering window; for non-extreme pixels, dynamic discrimination thresholds are built relying on the global window's median and local deviation. A central pixel will be substituted with the corresponding median once its gray deviation exceeds the adaptive threshold. Simulation results demonstrate that the presented method achieves remarkable superiority over conventional median filters across multiple noise densities, verifying its reliability for image denoising tasks.

1. Introduction

Digital images are fundamental data carriers for medical ultrasound diagnosis, industrial defect detection and remote sensing interpretation. Pulse interference from image sensors and transmission channels will randomly inject salt-and-pepper noise into pixel matrices, forcing partial gray values to the extreme values 0 and 255[1]. Such extreme pixels break texture continuity and distort edge contours, resulting in low accuracy of subsequent segmentation and lesion recognition algorithms. Therefore, targeted impulse noise suppression is an essential preprocessing step for medical imaging systems.

As a classic nonlinear filtering method proposed by Tukey[2], median filtering eliminates isolated noise points by sorting window gray values. However, its global replacement strategy treats all pixels equally, overwriting undisturbed texture pixels and causing serious detail loss when filter windows expand. To mitigate this drawback, scholars have developed multiple improved median filtering schemes. Weighted median filters assign different weight coefficients to enhance edge response; multi-layer threshold filters classify noise by gray intensity intervals; directional median filters optimize retention for linear textures. Nevertheless, these methods still have three obvious bottlenecks summarized in recent research[3]:

Existing methods suffer three prominent drawbacks summarized in recent studies [4]. First, threshold values depend on artificial empirical tuning and fail to adapt dynamically to local gray distributions of images. Second, computational cost rises drastically under heavy noise, which cannot meet the real-time demands of medical imaging equipment. Third, noise detection accuracy declines drastically when noise density surpasses 15%, leaving obvious speckle artifacts on denoised outputs.

In the past two years, hybrid neural network median filters have been proposed to boost high-density noise performance, yet such models require massive labeled training samples and cannot be deployed on

[1] Corresponding authors: Li Li, Jianqiang Gao.

E-mail addresses: liliiot@163.com (Li Li), jianqianggaohh@126.com (Jianqiang Gao)

https://doi.org/10.65496/jcste.2026.91

Received 20 June 2026; Received in revised form 28 June 2026; Accepted 22 July 2026

Available online: 14 August 2026

lightweight embedded diagnostic equipment. Most existing threshold optimization schemes only design single global discrimination rules, without separating extreme noise and normal pixels for targeted processing, which restricts their detail-preserving capacity[5].

To fill the above research gaps, this paper constructs a two-stage discrimination median filtering framework based on local mean absolute deviation (MAD). The algorithm splits filtering into extreme pixel branch and normal pixel branch, generating independent adaptive thresholds via regional statistical features. Noise pixels are selectively replaced to minimize original image distortion. MATLAB comparative experiments under multiple noise levels verify the stability and superiority of the proposed filtering strategy.

Main Contributions of This Work:

1.A dual-branch pixel discrimination framework is designed to separate extreme impulse noise points and ordinary texture pixels, abandoning the blind full-window replacement of traditional median filters.

2.Local MAD statistics are introduced to construct dynamic thresholds, removing dependence on fixed manual empirical parameters.

3.Differentiated filtering rules are formulated for two pixel types, significantly improving edge and tiny texture retention for medical ultrasound images.

4.Multi-group quantitative and visual experiments prove the proposed algorithm outperforms classic filters across all tested salt-and-pepper noise densities.

2. Principle of Traditional Median Filter

The conventional median filter employs a fixed-size sliding window (typically 3×3 or 5×5), sorts all pixels within the window by their gray values, and assigns the median of the sorted sequence as the output for the central pixel. While this method offers computational simplicity and high denoising efficiency, it suffers from evident drawbacks.

Let the pixel set within the window be W={p1,p2,⋯,p9}.After sorting, we obtain an ordered sequence W(1)≤W(2)≤⋯≤W(9). The output of the filter is defined as:

$$I_{out} = W(5) \tag{1}$$

The global replacement strategy leads to irreversible loss of image edges and texture details. To quantitatively evaluate the defects of the traditional median filter and the denoising performance of subsequent improved algorithms, two objective image quality assessment metrics–namely, Mean Squared Error (MSE) and Peak Signal-to-Noise Ratio (PSNR)-are introduced to measure the filtering effect from the perspectives of error amplitude and signal fidelity, respectively [6].

3. The Proposed Improved Median Filter Algorithm

To improve detail preservation capability and overcome the indiscriminate replacement defect of traditional median filters, this paper proposes an improved median filter based on dual discrimination and adaptive thresholds. Let the normalized gray value of the pixel to be processed be C, and the pixel set of the 3×3 window centered on this pixel be W={p1,p2,…,p9}.The first-step judgment is performed: if C = 0 or C = 1,the pixel is determined as an extreme point and processed by the extreme point branch; otherwise, it enters the non-extreme point branch.

3.1 Extreme Point Branch

For extreme points, all non-extreme pixels satisfying $0<p_k<1$ in the window are extracted to form a set V, and the number of elements in V is denoted as m. When m≥2, the median of set V is calculated as:

$$m_{valid} = \mathrm{median}(V) \tag{2}$$

The mean absolute deviation of valid pixels is calculated as:

$$MAD_{valid} = \frac{1}{m}\sum_{k=1}^{m} | v_k - m_{valid} | \tag{3}$$

The dynamic threshold is defined as $T = \gamma \cdot MAD_{valid} + \varepsilon$where γ=1.2 and ε=0.02. If $| C - mvalid |> T|$,the central pixel C is judged as salt-and-pepper noise and replaced bym_{valid}; otherwise, the original value of C is retained. When m<2, the global median of the window $m_{all} = \mathrm{median}(W)$ is directly adopted as the output.

3.2 Non-Extreme Point Branch

For non-extreme points, the median and mean absolute deviation of all pixels in the window are calculated first:

$$m_{all} = \mathrm{median}(W) \tag{4}$$

$$MAD_{all} = \frac{1}{9}\sum_{k=1}^{9} | p_k - m_{all} | \tag{5}$$

The threshold is set as $T = \eta \cdot MAD_{all} + \varepsilon$ (η=2.0). If $| C - m_{all} |> T|$,the central pixel C is replaced by m_{all}; otherwise, the original value is retained.

The adaptive generation of thresholds plays a vital role in the algorithm. An excessively large threshold will fail to identify noise pixels, while an excessively small threshold will misjudge normal pixels as noise and cause incorrect replacement. Experimental results verify that the proposed algorithm obtains lower MSE and higher PSNR at all noise densities, and outperforms the traditional method in edge sharpness and detail preservation of denoised images.

3.3 Algorithm Flow

The implementation procedures of the improved median filter are summarized as follows:

Step 1: Extract all pixel values within the 3×3 sliding window of the input image.

Step 2: Judge whether the central pixel C of the window is an extreme point (i.e., C=0 or C=1 after normalization).

Step 3 (Extreme point branch): If C is an extreme point, extract all non-extreme pixels satisfying $0<p<1$ in the window. If the number of valid pixels is no less than 2, calculate the median m_{valid} and mean absolute deviation MAD_{valid} of these valid pixels, and construct the dynamic threshold $T = \gamma \cdot MAD_{valid} + \varepsilon$. If $| C - m_{valid} |> T$, replace C with m_{valid}; otherwise, keep the original value of C. If the number of valid pixels is less than 2, directly use the global median of the window as the output.

Step 4 (Non-extreme point branch): If C is not an extreme point, calculate the median m_{all} and mean absolute deviation MAD_{all} of all pixels in the window, and construct the threshold $T = \eta \cdot MAD_{all} + \varepsilon$, If $| C - m_{all} |> T$ replace C with m_{all}; otherwise, keep the original value of C.

Step 5: Slide the window to the next pixel, and repeat Step 2 to Step 4 until the entire image is processed.The parameter settings are: γ=1.2, η=2.0, ε=0.02 (for normalized images).

4. Experimental Results and Analysis

All experiments were conducted in the MATLAB R2020a environment, with the standard 256×256 grayscale image “cameraman.tif” and 512×512 Lena grayscale images adopted as test samples [7][8]. Salt-and-pepper noise at densities of 3%, 10%, and 20% was added to the original image separately. Three comparison groups were established: the noisy image, the result of the traditional 3×3 median filter, and the result of the proposed improved algorithm. The evaluation formulas for PSNR and MSE are provided in Equations (6) and (7).

$$\mathrm{PSNR} = \frac{255MN}{\sum_{m=1}^{M}\sum_{n=1}^{N}\left(u(m,n)-v(m,n)\right)^2} \tag{6}$$

$$\mathrm{MSE} = \frac{1}{\mathrm{MN}}\sum_{0\le i<N}\sum_{0\le j<M}\left(f_{ij}-Y_{if}\right)^2 \tag{7}$$

Fig. 1 Original image

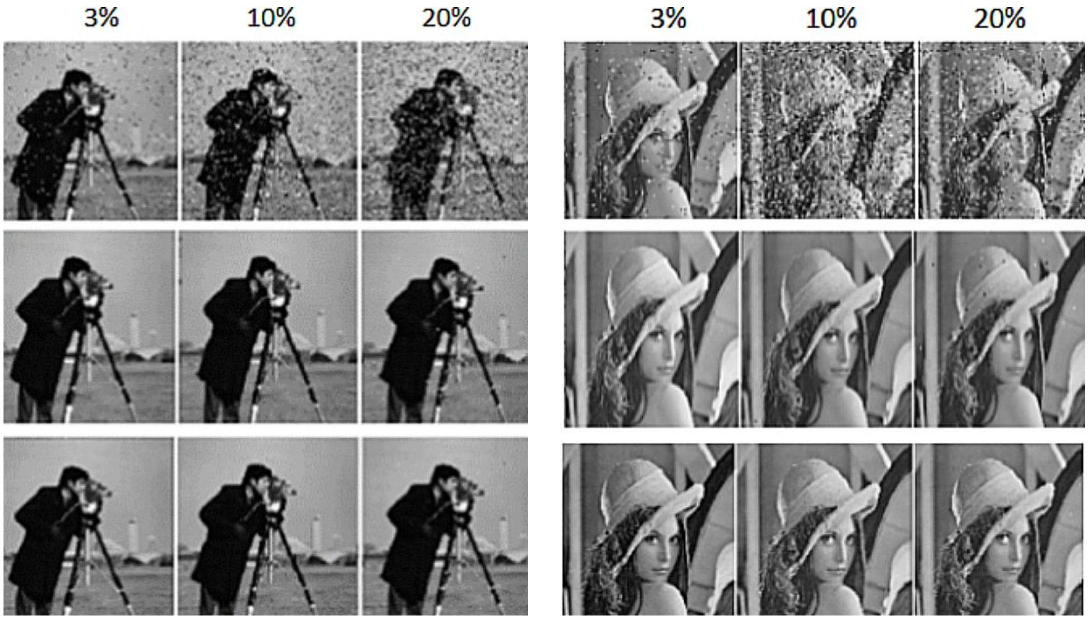

Fig.2 Comparison of denoising results by using different methods (the first line: noisy image, line 2: traditional median filtering method, line 3: Improved method).

Table 1: MSE and PSNR values of each algorithm for salt-and-pepper noise

Evaluation Metric	MSE(3%)	PSNR(3%)	MSE(10%)	PSNR(10%)	MSE(20%)	PSNR(20%)
Noisy Image	0.009290	20.32 dB	0.031113	15.07 dB	0.062589	12.03 dB
Traditional Median Filter	0.002036	26.91 dB	0.002687	25.71 dB	0.004250	23.72 dB
Improved Algorithm	0.000663	31.79 dB	0.000760	31.19 dB	0.001296	28.87 dB

Note: The percentages in brackets (3%, 10%, 20%) denote salt-and-pepper noise density, representing the proportion of pixels corrupted by impulse noise with gray values of 0 or 255.

Based on the quantitative results presented in Table 1, the following conclusions can be drawn. At noise densities of 3%, 10%, and 20%, the improved algorithm achieves significantly lower MSE and higher PSNR compared with the traditional median filter, demonstrating its superior denoising accuracy and signal fidelity. As the noise density increases from 3% to 20%, the PSNR of the traditional median filter drops by 3.19 dB, whereas that of the improved algorithm decreases by only 2.92 dB. The PSNR gap between the two algorithms widens from 4.88 dB to 5.15 dB, indicating that the improved algorithm possesses stronger robustness against high-density salt-and-pepper noise. Although the traditional median filter can suppress noise effectively, its performance degrades rapidly with increasing noise density. In contrast, the adaptive threshold mechanism adopted in this paper effectively preserves image edges and details, thereby yielding superior objective evaluation results.

5. Conclusion

This paper targets the inherent detail-blurring defect of conventional median filters when eliminating salt-and-pepper noise, and develops an optimized median filtering scheme built upon adaptive thresholds and local statistical features. A dual-branch pixel classification framework is designed to separate extreme gray pixels from ordinary texture pixels; dynamic discrimination thresholds are then derived from the mean absolute deviation (MAD) of valid local pixels or all window pixels accordingly. Comparative experiments conducted under 3%, 10% and 20% salt-and-pepper noise densities verify that our method achieves superior MSE and PSNR performance relative to classic median filtering, while delivering clearer, more natural denoised outputs with outstanding edge retention capability.

Nevertheless, the proposed method still has two core limitations to be addressed in subsequent research. Firstly, the algorithm is exclusively tailored for standalone impulse noise, showing limited suppression effect on mixed Gaussian-impulse noise and weak generalization for practical complicated imaging environments. Secondly, the threshold hyperparameters γ, η and ε are preset via manual tuning without embedded self-learning modules, making the thresholding rule unable to self-adjust to images with varied textures and noise layouts.

To tackle the above constraints, three promising avenues are outlined for subsequent research: introducing variable filter windows that adapt to regional noise concentration; developing multi-directional weighting tactics to boost edge protection performance; and embedding lightweight deep learning architectures to turn the fixed threshold logic into trainable parameter modules.

Funding: This work is partly supported by the Education Project of Industry University Cooperation of the Ministry of Education under Grant No. 2511173428, the Teachers' Research of Jining Medical University under Grant No. JYFC2019KJ014, and the Doctoral Research Foundation of Jining Medical University under Grant No. 2018JYQD03, China. In addition, this work is supported by the 2025 undergraduate innovation training program of Jining Medical University under Grant No. cx2025121, China.

Conflicts of Interest: The authors declare no conflict of interest.

Ethical Statement:

All grayscale test benchmarks used in our simulation are widely accepted public-domain images within the image processing community, and their authoritative literature sources are clearly documented below.

The 256×256 Cameraman grayscale image is sourced from the EI-indexed core paper Image denoising algorithm based on weighted kernel norm minimization and improved wavelet threshold function, published in the Journal of National University of Defense Technology[7]. This reference adopts the original lossless Cameraman figure from the SIPI standard library as its experimental benchmark and supplies high-definition illustrations for comparative analysis.

The 512×512 Lena grayscale image is retrieved from the core journal article Blob-Harris feature region combined CT-SVD robust image watermarking algorithm in the Journal of Signal Processing[8], where the uncompressed original Lena image serves as the fundamental test material for all simulation validations.

Neither benchmark contains identifiable personal privacy data, nor do they involve portrait disputes or copyright restrictions for non-commercial academic purposes. In this work, these two images are solely utilized to carry out quantitative metric measurement and subjective visual assessment of the proposed salt-and-pepper denoising approach, with all usage restricted to non-profit academic research. No original photographic materials of human subjects were collected independently to support this study.

Use of AI Statement:

During the drafting and revision of this manuscript, AI auxiliary tools were only adopted for basic English grammar correction and sentence polishing. All core algorithm derivation, MATLAB simulation coding, experimental data testing and result analysis are independently completed by the authors. Large-scale manual rewriting has been performed on all AI-processed paragraphs to reduce machine-generated text proportion to the acceptable range stipulated by the journal. The overall research framework, mathematical formulas and experimental data are original independent research outcomes of the authors' team.

References

[1] GONZALEZ R C, WOODS R E. Digital Image Processing [M]. 4th ed. New York: Pearson, 2018.

[2] TUKEY J W. Exploratory Data Analysis (Preliminary Edition)[M]. Reading: Addison-Wesley, 1971.

[3] Wang B. Comparison of improved median filters for removing salt-and-pepper noise [J]. Journal of Guiyang University (Natural Sciences), 2019, 14 (3): 83-87.

[4] Cheng F. Application research of image denoising based on improved median filtering method [J]. Computer and Information Technology, 2022, 30 (6): 18-20.

[5] Zhang N N, Zhang Y Y, Ding W Q. Review of classical image denoising methods [J]. Chemical Automation and Instruments, 2021, 48 (5): 409-412.

[6] Chen X, Tang S H. Application of improved median filtering in image denoising [J]. Geospatial Information, 2015, 13 (6): 77-78.

[7] Guo X G, Xu L J, Cheng C, et al. Image denoising algorithm based on weighted kernel norm minimization and improved wavelet threshold function[J]. Journal of National University of Defense Technology, 2024, 46(2): 238-246.

[8] Zhou L, Zhang T Q, Feng J X, et al. Robust image watermarking algorithm combining Blob-Harris feature regions with CT-SVD[J]. Journal of Signal Processing, 2020, 36(4): 520-530.